

# Non-monotonic flow curves of shear thickening suspensions

Romain Mari and Ryohei Seto

*Benjamin Levich Institute, City College of New York, New York, NY 10031, USA*

Jeffrey F. Morris and Morton M. Denn

*Benjamin Levich Institute, City College of New York, New York, NY 10031, USA and  
Department of Chemical Engineering, City College of New York, New York, NY 10031, USA*

(Dated: August 18, 2018)

The discontinuous shear thickening (DST) of dense suspensions is a remarkable phenomenon in which the viscosity can increase by several orders of magnitude at a critical shear rate. It has the appearance of a first order phase transition between two hypothetical “states” that we have recently identified as Stokes flows with lubricated or frictional contacts, respectively. Here we extend the analogy further by means of novel stress-controlled simulations and show the existence of a non-monotonic steady-state flow curve analogous to a non-monotonic equation of state. While we associate DST with an S-shaped flow curve, at volume fractions above the shear jamming transition the frictional state loses flowability and the flow curve reduces to an arch, permitting the system to flow only at small stresses. Whereas a thermodynamic transition leads to phase separation in the coexistence region, we observe a uniform shear flow all along the thickening transition. A stability analysis suggests that uniform shear may be mechanically stable for the small Reynolds numbers and system sizes in a rheometer.

## I. INTRODUCTION

The shear thickening of dense suspensions is a counter-intuitive phenomenon in which, for some range of applied shear stress, the viscosity of a suspension increases, sometimes by orders of magnitude [1–3]. It is observed in systems that differ widely in the shape, type or size of the suspended solid material, or in the type of suspending liquid; it is even argued that most dense suspensions shear thicken, but the phenomenon may often be hidden by a yield stress [4, 5]. Despite being an inherently non-equilibrium phenomenon, shear thickening shares some strong similarities with an equilibrium phase transition. In Fig. 1 we show schematically the relation between the shear stress  $\sigma$  and the shear rate  $\dot{\gamma}$  as it is commonly observed in experiments [3, 6–9]. The curves observed at different volume fractions  $\phi$  are reminiscent of the isotherms in a  $P$ - $V$  diagram for a system undergoing a liquid-gas transition. This leads to an analogy between discontinuous shear thickening (DST) and a first order transition.

Along this line of thought, Wyart and Cates [10] recently suggested that a non-monotonic flow curve  $\dot{\gamma}(\sigma)$ , as represented in Fig. 1, underlies the discontinuity region, just as a first order transition stems from a non-monotonic equation of state. (The hypothesis of an S-shaped flow curve is controversial [11, 12]. The arguments of Wyart and Cates [10] rely on an interpolation between two hypothetical coexisting states, one frictionless and one frictional.) For the liquid-gas transition, the S-shaped equation of state is never observed even in a volume-controlled experiment, because it leads to a coexistence region where the uniform system is no longer a global minimum of the free energy and the system phase separates. For DST, however, one cannot rely on a thermodynamic argument and we are restricted to mechan-

ical considerations. For micellar systems, a mechanical stability analysis of the “spinodal” region (the region inside the coexistence region with  $d\dot{\gamma}/d\sigma < 0$ ) leads to an instability of the uniform flow towards shear banding, which is a mechanical phase separation [13, 14]. Interestingly, even if many DST experiments show the “thermodynamic” behavior described in Fig. 1, with a shear rate plateau in the discontinuity region under stress-controlled conditions, some experiments instead show a non-monotonic rheology [15–17], and a very recent study [11] clearly maps out a full S-shaped curve for a neutrally buoyant suspension of spheres, but with hysteresis and a rate dependence of the transition in the flow curve. Some related granular flows have been studied at fixed shear stress and showed a similar non-monotonic  $\dot{\gamma}(\sigma)$  relation, but only as a transient [18].

Here we address these properties of DST and non-monotonicity with numerical simulations of a model shear-thickening suspension of hard frictional spherical particles. The simulation model, which considers frictional contacts between suspended particles, has recently been shown to reproduce both continuous shear thickening (CST) and DST under rate control, as observed in experiments [19–22]. Modern shear rheology experiments are often carried out under shear stress rather than shear rate control, but existing methods to simulate stress-controlled flows of dense suspensions, by introducing walls or feedback loops, are of limited utility and cannot be used to simulate DST. We describe here a novel deterministic stress-controlled scheme employing periodic boundary conditions that makes it possible for the first time to simulate the flow in the DST regime. We observe both the S-shaped flow curves and the arches suggested by analogy to a first order transition (cf. Fig. 1) *in steady state with a uniform flow*; there is no mechanical instability leading to shear-banding or chaotic dynam-

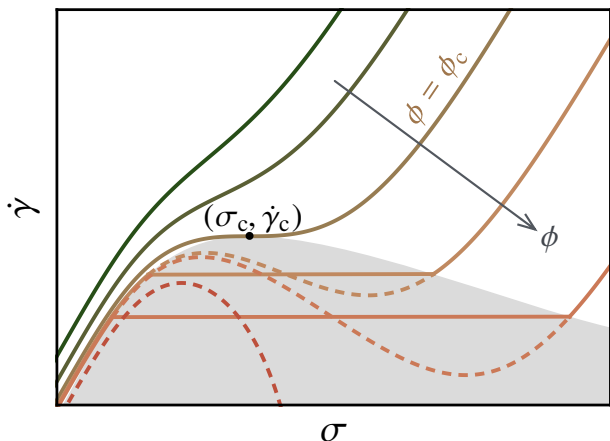


FIG. 1. (Color online). Sketch of the relation between the shear rate  $\dot{\gamma}$  and the shear stress  $\sigma$  in a shear thickening suspension, with increasing volume fraction  $\phi$  from top to bottom, in solid lines. At low  $\phi$ ,  $\dot{\gamma}(\sigma)$  is a strictly monotonic function and the shear thickening is continuous, appearing as an inflection in the curve. As  $\phi$  increases, this inflection deepens, and at  $\phi = \phi_c$  a “critical” point  $(\sigma_c, \dot{\gamma}_c)$  appears in which  $d\dot{\gamma}/d\sigma = 0$ . For  $\phi > \phi_c$  the shear thickening is discontinuous. The discontinuity region (with constant  $\dot{\gamma}$ ) is analogous to a coexistence region (light gray region). (Hysteresis is sometimes observed, in which case the discontinuity region would be analogous to a spinodal region.) The discontinuity region is only accessible under stress-controlled conditions. The putative non-monotonic flow curves are plotted as dashed lines in the coexistence region, in analogy to the non-monotonic equations of state underlying a first order thermodynamic transition.

ics [23], in stark contrast to a thermodynamic transition.

## II. METHODS

We simulate an assembly of inertialess frictional spheres immersed in a Newtonian fluid under simple shear flow. The system is binary, with radii  $a$  and  $1.4a$  mixed at equal volume fractions. A stabilizing repulsive force that prevents frictional contacts between particles at low stresses, as used in our basic model [21], is a key ingredient in shear thickening; in many shear thickening experiments this takes the form of an electrostatic double-layer force [15]. The equation of motion is thus simply the force balance between hydrodynamic ( $\mathbf{F}_H$ ), repulsive ( $\mathbf{F}_R$ ), and contact ( $\mathbf{F}_C$ ) forces which depend on the many-body position and velocity vectors  $\mathbf{X}$  and  $\mathbf{U}(\equiv \dot{\mathbf{X}})$ :

$$\mathbf{0} = \mathbf{F}_H(\mathbf{X}, \mathbf{U}) + \mathbf{F}_R(\mathbf{X}) + \mathbf{F}_C(\mathbf{X}). \quad (1)$$

The hydrodynamic forces consist of two components, a drag due to the motion relative to the surrounding fluid,  $-\mathbf{R}_{\text{FU}}(\mathbf{X}) \cdot (\mathbf{U} - \mathbf{U}^\infty)$ , and a resistance to the deformation imposed by the flow,  $\dot{\gamma} \mathbf{R}_{\text{FE}} : \hat{\mathbf{E}}^\infty$ , where

$\mathbf{U}_i^\infty = \dot{\gamma} y_i \hat{\mathbf{e}}_x$  and  $\hat{\mathbf{E}}^\infty \equiv (\hat{\mathbf{e}}_x \hat{\mathbf{e}}_y + \hat{\mathbf{e}}_y \hat{\mathbf{e}}_x)/2$  is the normalized strain rate tensor. (In very dense suspensions, the use of  $\mathbf{U}^\infty$  to model the effect of the surrounding fluid is unclear [24].  $\mathbf{U}^\infty$  tends to reduce the fluctuations around the homogeneous flow, but we have established that our results are unchanged if we remove this term, which is much smaller than the lubrication and contact forces.) The resistance matrices  $\mathbf{R}_{\text{FU}}$  and  $\mathbf{R}_{\text{FE}}$  contain the Stokes drag and the leading terms of the pairwise hydrodynamic lubrication interaction regularized to allow contacts [22, 25]. Contacts are modeled by a linear spring consisting of both normal and tangential components, with spring constants  $k_n$  and  $k_t$ , a simple model commonly used in granular physics [22]. In contrast to most granular physics models, however, there is no dashpot in our contact model, as the energy dissipation is provided by the hydrodynamic resistance. The electrostatic repulsion decays exponentially with the interparticle gap  $h$  as  $|\mathbf{F}_R| = F^* \exp(-h/\lambda_D)$ , with a Debye length  $\lambda_D$ .

The equation of motion (1) is completed by the constraint of flow at constant shear stress  $\sigma$ . At any time, the stress in the suspension is given by:

$$\sigma = \dot{\gamma} \eta_0 \left( 1 + \frac{5}{2} \phi \right) + \dot{\gamma} \eta_E + \sigma_R + \sigma_C \quad (2)$$

with  $\eta_0$  the suspending fluid viscosity,  $\eta_E = V^{-1} \{ (\mathbf{R}_{\text{SE}} - \mathbf{R}_{\text{SU}} \cdot \mathbf{R}_{\text{FU}}^{-1} \cdot \mathbf{R}_{\text{FE}}) : \hat{\mathbf{E}}^\infty \}_{xy}$  and  $\sigma_{R,C} = V^{-1} (\mathbf{X} \mathbf{F}_{R,C} - \mathbf{R}_{\text{SU}} \cdot \mathbf{R}_{\text{FU}}^{-1} \cdot \mathbf{F}_{R,C})_{xy}$ , where  $\mathbf{R}_{\text{SU}}$  and  $\mathbf{R}_{\text{SE}}$  are resistance matrices giving the lubrication stresses from the particles’ velocities and resistance to deformation, respectively [22, 26] and  $V$  is the volume of the simulation box. At fixed shear stress  $\sigma$  the shear rate  $\dot{\gamma}$  is the fluctuating variable that is to be determined at each time step by

$$\dot{\gamma} = \frac{\sigma - \sigma_R - \sigma_C}{\eta_0 \left( 1 + 2.5\phi \right) + \eta_E}. \quad (3)$$

The full solution of the equation of motion (1) under the constraint of fixed stress (2) is thus the following velocity  $\mathbf{U}$ :

$$\mathbf{U} = \mathbf{U}^\infty(\dot{\gamma}) + \mathbf{R}_{\text{FU}}^{-1} \cdot (\dot{\gamma} \mathbf{R}_{\text{FE}} : \hat{\mathbf{E}}^\infty + \mathbf{F}_R + \mathbf{F}_C). \quad (4)$$

We emphasize here that the stress control is *deterministic*, in the sense that the shear rate can be computed *a priori*, before applying the time step. This is a substantial advantage over the common technique of stress control using feedback, which adapts the shear rate based on the results of previous time steps. In particular, we do not have to introduce the relaxation time of the feedback loop as an additional time scale, and the shear stress of the system is strictly constant along the simulation. Boundary effects like layering are avoided by the use of periodic boundary conditions. It is also interesting to note that the time evolution (3) and (4) is valid even in a jammed state: we can have  $\dot{\gamma} = 0$  and  $\mathbf{U} = \mathbf{0}$  if  $\sigma = \sigma_R + \sigma_C$  and  $\mathbf{F}_R + \mathbf{F}_C = \mathbf{0}$ . Lastly, the unit scale is  $\dot{\gamma}_0 \equiv F^*/6\pi\eta_0 a^2$  for the strain rate and  $\sigma_0 \equiv \eta_0 \dot{\gamma}_0$  for the stress.

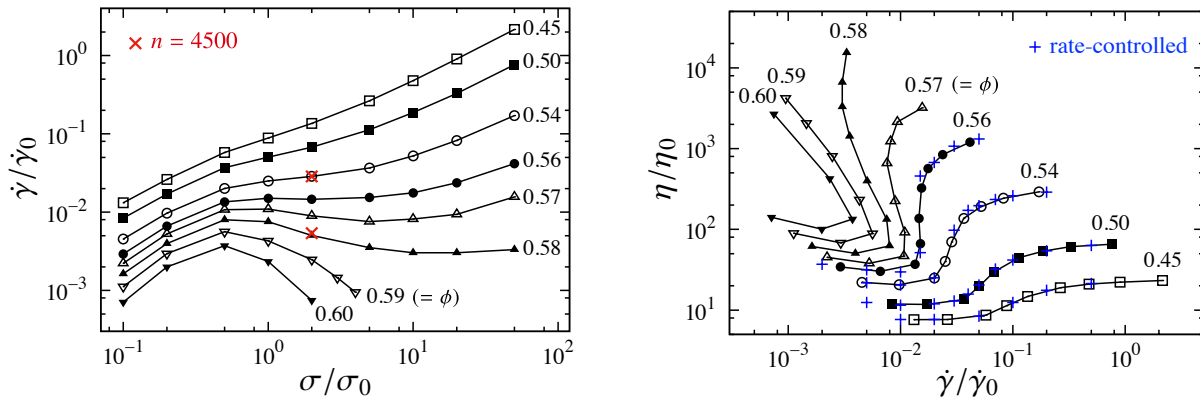


FIG. 2. (Color online) **Left:** The shear rate  $\dot{\gamma}$  as a function of the shear stress  $\sigma$  for several values of the volume fraction  $\phi$  in our simulations at constant shear stress. Continuous shear thickening at the lowest  $\phi$  is associated with monotonic flow curves, discontinuous shear thickening appears here as an S-shaped flow curve for  $\phi = 0.56$ – $0.58$ , and shear jamming is indicated by arch-shaped flow curves with a vanishing shear rate at high stresses for  $\phi \geq 0.59$ . Simulations are run with  $n = 500$  particles except for  $\phi = 0.58$ , for which we use  $n = 2000$ . Two data points with  $n = 4500$ , corresponding to the systems shown in Fig. 3, are indicated by red crosses. **Right:** The same data plotted as viscosity  $\eta$  versus shear rate  $\dot{\gamma}$  are compared with simulations at constant shear rate (blue crosses).

### III. RESULTS

In Fig. 2, we show the average shear rate as a function of the shear stress for several volume fractions  $\phi$ . At the lowest values of  $\phi$  the  $\dot{\gamma}(\sigma)$  curves are monotonic and show a continuous shear thickening for  $1 \lesssim \sigma/\sigma_0 \lesssim 10$ . The flow curve becomes non-monotonic at  $\phi = 0.56$ , and for  $\phi = 0.57$  and  $0.58$  the negative slope for intermediate stresses is clearly visible, showing that an S-shaped rheology curve lies behind the discontinuous shear thickening observed at the same volume fraction under a rate controlled simulation. Lastly, for  $\phi > 0.58$ , the flow curves are arches and the system flows only for small values of the stress, as the shear rate vanishes above a stress  $\sigma_{\max}(\phi)$ . For  $\sigma > \sigma_{\max}(\phi)$  the system cannot flow; it is in a shear jammed state, similar to the one observed in granular systems [27]. In our shear jammed states, the entire stress is supported by the repulsive and contact forces and particles have vanishing velocities. Unlike in a dry granular material, however, the system flows again in steady state with a subsequent decrease in stress for  $\sigma < \sigma_{\max}(\phi)$ . (There is also a yield stress above which the system flows again, due to the deformation of the particles under shear, but this stress scale is significantly larger than  $\sigma_{\max}(\phi)$  and we have not probed it.) This phenomenology is also present for the viscosity  $\eta$  as a function of  $\dot{\gamma}$  plotted in the right side of Fig. 2, which shows the same non-monotonicity for  $\phi \gtrsim 0.56$ . The calculations at constant shear rate are also shown, and the two sets agree very well out of the DST transition zone.

The system shows no sign of spatial heterogeneity within the  $d\dot{\gamma}/d\sigma < 0$  region, and the uniform shear flow is preserved. In the upper panel of Fig. 3 we plot the instantaneous velocity profile at a stress  $\sigma/\sigma_0 = 2$  for

$\phi = 0.54$  and  $\phi = 0.58$ ; both are in the shear thickening regime, but with  $d\dot{\gamma}/d\sigma > 0$  for  $\phi = 0.54$  and  $d\dot{\gamma}/d\sigma < 0$  for  $\phi = 0.58$ . The velocity profile is linear across the sample in both cases, indicating a uniform flow. The normalized fluctuations around the mean flow at particle level,  $|\mathbf{U}_i - \mathbf{U}_i^\infty|/\dot{\gamma}a$ , are shown as color-coded snapshots in the lower panel of Fig. 3. These normalized fluctuations are larger for the denser  $\phi = 0.58$  than for  $\phi = 0.54$  (they may actually diverge with the viscosity at the jamming transition, as a dissipation argument shows [28]), but they do not show any structure associated with a phase separation. Neither do they show large fluctuations in the time series, as has been observed in some experiments [16]. We show the strain series of the shear rate for three system sizes in the negative slope region in Fig. 4. The variance of the shear rate decreases with increasing system size  $n$ , and there is no sign of intermittency or macroscopically chaotic behavior. This indicates that the uniform shear is the steady state in this region.

### IV. STABILITY ANALYSIS

For micellar systems, where one can observe a similar decreasing flow curve, the uniform flow is mechanically unstable against perturbations of the velocity field along the flow direction due to inertia if  $\dot{\gamma}$  and  $\sigma$  are instantaneously related through a decreasing flow curve [13, 14, 29, 30]. Our simulations are strictly inertialess, so it is natural to address the question of the validity of our results for the small but finite inertia observed in experiments. We carry out a linear stability analysis at a simplified scalar level for a suspension at a volume fraction  $\phi$  and shear stress  $\sigma$  within the decreasing region of

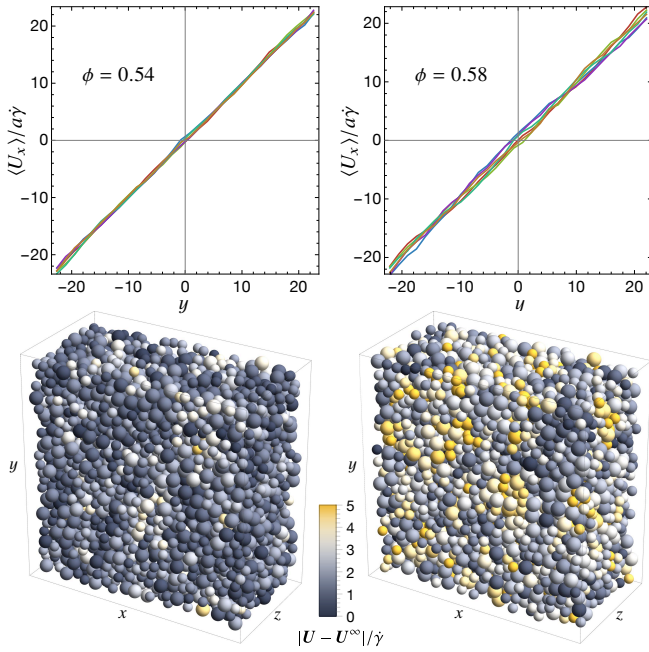


FIG. 3. (Color online) **Top:** Instantaneous velocity profiles in the shear thickening regime ( $\sigma/\sigma_0 = 2$ ) for  $\phi = 0.54$  (left), where  $d\dot{\gamma}/d\sigma > 0$ , and for  $\phi = 0.58$  (right), where  $d\dot{\gamma}/d\sigma < 0$ . The different curves are taken at different strains separated by one strain unit. In both cases the shear flow is uniform. **Bottom:** Configurations of the system at  $\phi = 0.54$  (left) and  $\phi = 0.58$  (right) and stress  $\sigma/\sigma_0 = 2$  as above, color coded with the norm of the non-affine velocity, from dark gray (small value) to yellow (light gray, large value). Fluctuations are larger at higher volume fraction, but they do not show any sign of non-uniform flow or phase separation.

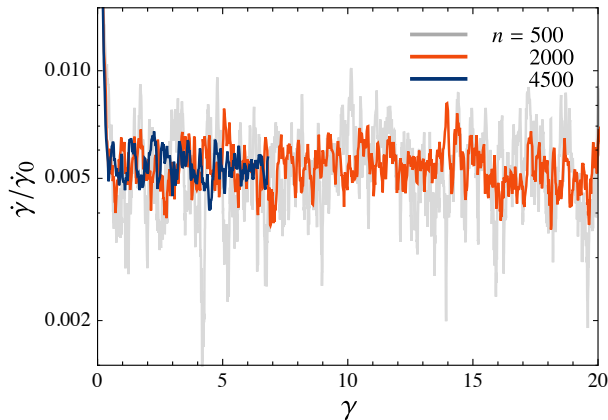


FIG. 4. (Color online) Strain series of the shear rate for  $\phi = 0.58$  and  $\sigma/\sigma_0 = 2$ , for which the steady state flow curve shows  $d\dot{\gamma}/d\sigma < 0$ . The system shows no intermittency or exotic fluctuating or chaotic behavior and is in a simple steady state. Three sizes are shown:  $n = 500, 2000, 4500$ , from which we can see that the variance of the signal decreases with increasing  $n$ , as is expected for a steady uniform shear flow.

the flow curve, i.e., where  $d\dot{\gamma}/d\sigma < 0$ . We show that the system is linearly stable to perturbations along the flow direction for small Reynolds numbers and finite system sizes because of a delay inherent to the microstructural reorganization in the suspension. (This analysis is close in spirit to the analysis provided by Nakanishi *et al.* [23] for an effective hydrodynamic model of shear thickening fluids, and it leads to similar conclusions.)

We perform a stability analysis of the momentum equation:

$$\rho \left( \frac{\partial \mathbf{v}}{\partial t} + \mathbf{v} \cdot \nabla \mathbf{v} \right) = \nabla \cdot \boldsymbol{\Sigma} \quad (5)$$

that we restrict to simplified scalar (one-dimensional) perturbations. The unperturbed velocity profile is uniform  $\mathbf{v}(\mathbf{r}) = \dot{\gamma}^* y \hat{\mathbf{e}}_x$  and it is associated with a constant shear stress field  $\boldsymbol{\Sigma}_{xy}(\mathbf{r}) = \sigma^*$ . We introduce a perturbation  $\delta v(y, t) \hat{\mathbf{e}}_x$  in the velocity field and  $\delta \sigma(y, t)$  in the stress field. As  $\mathbf{v} \cdot \nabla \mathbf{v} = 0$ , the momentum equation becomes:

$$\rho \frac{\partial \delta v}{\partial t} = \frac{\partial \delta \sigma}{\partial y}. \quad (6)$$

We then need a relation between the  $\sigma$  and  $\dot{\gamma}$  that is valid at any time. If these quantities are linked through their steady state relation  $\dot{\gamma}^*(\sigma)$  (that is, if the relaxation time is strictly zero), the uniform flow is unstable whenever  $d\dot{\gamma}^*/d\sigma < 0$  [14]. However, these two quantities are actually linked through the microstructure of the system: the number of frictional contacts and their anisotropy directly affect the relation between  $\dot{\gamma}$  and  $\sigma$ . When there is a local perturbation the microstructure response requires strain to evolve. To a first approximation, we can account for this microstructural effect through a scalar variable  $f$ , the fraction of frictional contacts, such that at any time the viscosity (at fixed volume fraction) is a unique function  $\eta(f)$  [10, 22]. Building or destroying the contact network takes strain, and  $f(y, t) = f^* + \delta f(y, t)$  can be assumed to evolve in the linear regime as

$$\delta f(y, t) = \int_{-\infty}^{\gamma(t)} d\gamma' K(\gamma - \gamma') \delta \sigma(y, \gamma'), \quad (7)$$

where  $K$  is a memory kernel that depends on the initial steady state stress  $\sigma^*$ . Changing the variable of integration to time and using the fact that  $\delta \sigma = \delta \eta \dot{\gamma}^* + \eta^* \delta \dot{\gamma}$ , we then have at linear order:

$$\delta \sigma = \eta^* \delta \dot{\gamma} + \dot{\gamma}^{*2} \frac{d\eta^*}{df} \int_{-\infty}^t dt' K(\dot{\gamma}^*(t - t')) \delta \sigma(t'). \quad (8)$$

Now, assuming a periodic perturbation  $\delta v(y, t) = w(t) e^{iky}$  and  $\delta \sigma(y, t) = r(t) e^{iky}$ , taking the Laplace transform of (8) and (6), we have:

$$\hat{r}(s) = \frac{ik\eta^* w(0)}{s + k^2 \eta^* / \rho - s \dot{\gamma}^* (d\eta^*/df) \hat{K}(s/\dot{\gamma}^*)} \quad (9)$$

with  $\hat{r}(s)$  and  $\hat{K}(s)$  the Laplace transforms of  $r(t)$  and  $K(t)$ . The final value theorem states that  $r(t)$  vanishes when  $t \rightarrow \infty$  if  $\hat{r}(s)$  has no singularity in the right half of the complex plane, that is, if  $s + k^2\eta^*/\rho - s\dot{\gamma}^*(d\eta^*/d\sigma)\hat{K}(s/\dot{\gamma}^*)$  has no roots with positive real part.

In the simple case of an exponential kernel  $K(t) = K'e^{-c\dot{\gamma}^*t}$  (with  $K' = cdf^*/d\sigma$ ), we are thus looking at solutions of:

$$s + \frac{k^2\eta^*}{\rho} - \dot{\gamma}^*c \frac{d\eta^*}{d\sigma} \frac{s}{s/\dot{\gamma}^* + c} = 0, \quad (10)$$

which is a quadratic equation with solutions  $s_1$  and  $s_2$  satisfying:

$$s_1 s_2 > 0, \quad s_1 + s_2 = -\eta^* \dot{\gamma}^* c \frac{d\dot{\gamma}^*}{d\sigma} - \frac{k^2\eta^*}{\rho}, \quad (11)$$

meaning that the real parts of both roots are negative if  $d\dot{\gamma}^*/d\sigma > -k^2/(\rho\dot{\gamma}^*c)$ . However, when  $d\dot{\gamma}^*/d\sigma < -k^2/(\rho\dot{\gamma}^*c)$ , the roots have a positive real part, which means that the uniform shear flow is unstable. This stems from the competition between the time needed to build a microstructure  $(\dot{\gamma}^*c)^{-1}$  (the longer the more stable) and the damping time  $\rho/(k^2\eta^*)$  on a length scale  $k^{-1}$  (the longer the more unstable). In the thermodynamic limit the wave-vector  $k$  can take arbitrarily small values and the uniform shear flow will be unstable whenever  $d\dot{\gamma}^*/d\sigma < 0$ . However if the flow occurs in a finite gap  $H$  the smallest wave vector available is  $k = \pi/H$  and the uniform shear flow is stable for Reynolds numbers  $\text{Re} \equiv \rho\dot{\gamma}^*H^2/\eta^*$  smaller than a critical  $\text{Re}_c$ :

$$\text{Re}_c = -\frac{\pi^2}{c\eta^*} \left( \frac{d\dot{\gamma}^*}{d\sigma} \right)^{-1}. \quad (12)$$

Note that for the simulations shown in this article, the stability is provided not by the finite size of the system, but by the fact that the inertia is strictly neglected and  $\text{Re} = 0$ .

In order to understand this stability from a physical point of view, we can consider the case of a step increase of the shear stress at a given strain  $\gamma^{\text{step}}$ , so that  $\sigma(\gamma) = \sigma^* + \Theta(\gamma - \gamma^{\text{step}})\delta\sigma$ , for a stress  $\sigma^*$  in the region  $d\dot{\gamma}^*/d\sigma < 0$ . Using (6)-(8) and , we find that whereas the local microstructure variable and the viscosity respond monotonically to the shear stress increase, the shear rate does not: it first increases before relaxing to its steady state value as  $\dot{\gamma}(\gamma) = \dot{\gamma}^* + \left[ (d\dot{\gamma}^*/d\sigma) \left( 1 - e^{-c(\gamma - \gamma^{\text{step}})} \right) + e^{-c(\gamma - \gamma^{\text{step}})}/\eta^* \right] \Theta(\gamma - \gamma^{\text{step}})\delta\sigma$ . As shown in Fig. 5, this nonmonotonic response is observed in our simulations: following a step increase in stress, the shear rate, initially at  $\dot{\gamma}^*$ , immediately jumps to a higher value before decreasing to its steady state value  $\dot{\gamma} < \dot{\gamma}^*$  in a relaxation that is reasonably fit by an exponential decay with strain scale  $c^{-1} = 0.023$  (i.e. 2.3%). This can be understood if we decompose the stress response: the stress increase in the bulk just after the perturbation at  $\gamma = \gamma^{\text{step}}$  cannot have

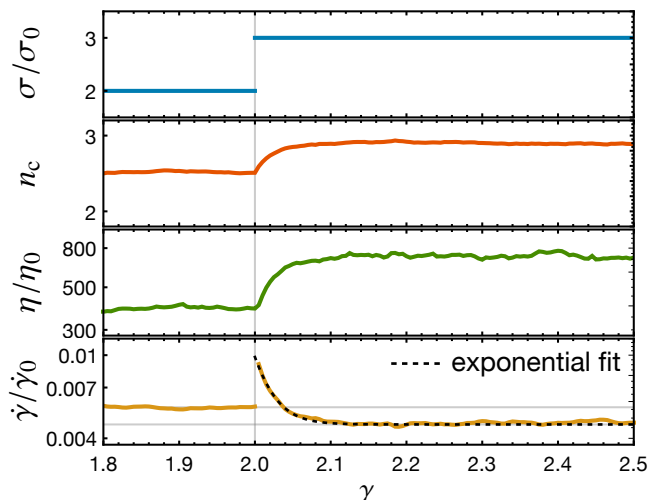


FIG. 5. (Color online) Typical strain response to a step increment of applied stress in the region  $d\dot{\gamma}^*/d\sigma < 0$ . These curves are obtained by averaging 100 simulations at  $\phi = 0.58$ , for which we impose a stress  $\sigma/\sigma_0 = 2$  for strains  $\gamma < 2$  and increment to  $\sigma/\sigma_0 = 3$  at  $\gamma = 2$  (top panel). The average contact number per particle  $n_c$  and the viscosity  $\eta$  increase (middle panels), with an exponential-like relaxation, but the shear rate  $\dot{\gamma}$  has a non-monotonic behavior, first increasing and then relaxing to a lower value (bottom panel). The dashed line is a fit to an exponential relaxation, giving a relaxation strain of  $c^{-1} \approx 0.023$  for these conditions. Hence at short time scales, and in particular on the inertial time scale, the shear rate increases with the shear stress and the system is mechanically stable.

its origin from contacts, because the microstructural reorganization needed to accommodate the stress change through a contact network takes time to build up. The initial stress response is of hydrodynamic origin, and this component of the stress increases only upon an increase of the shear rate. As a consequence, if the Reynolds number is small enough, on the inertial time scale the suspension always behaves like a stable fluid that flows faster with increased applied stress.

## V. DISCUSSION

Our numerical simulations and the linear stability analysis indicate that it may be possible to observe the S-shaped rheology in experiments, and S-shaped flow curves have recently been observed for a neutrally-buoyant suspension of spheres [11], although the simulation does not capture the hysteresis and rate-dependent onset of the re-entrant portion of the flow curve seen in these experiments. In some stress-controlled experiments the DST shows up in the  $\dot{\gamma}(\sigma)$  curve as an intermediate plateau with  $d\dot{\gamma}/d\sigma = 0$ . The Reynolds numbers involved in these experiments are often within the range for which our stability analysis predicts a stable uniform shear flow, so deep stable S-shaped flow curves would be noticed in

the experimental data. For polymer beads in glycol [15] and comb polymer coated PMMA beads in various organic solvents [16] at volume fractions similar to the ones studied in this article, experiments show first a decrease and then a plateau for the shear rate above the discontinuous shear thickening onset stress. For precipitated calcium carbonate suspensions, a linear decrease of the shear rate is sometimes observed [31, 32]. A recent experiment on fluidized gypsum suspensions in water [17] shows the arching flow curves associated with shear jamming resembling the ones we obtain in this work for  $\phi > 0.58$ . It then seems that the decreasing flow curve is stable under some conditions, but that most of the time it is hidden by another phenomenon leading to a shear rate plateau.

Our stability analysis is highly restrictive, and the absence of non-monotonic flow curves in some experiments could be a consequence of another type of instability. To this end, a stability analysis extended to at least two dimensions would be valuable, but for now we are limited by the rather simplistic constitutive connection between the microstructure and the rheology. Furthermore, the “order parameter”  $f$  is a scalar, and we neglect the vol-

ume fraction field and its fluctuations. Finally, another important point may be the neglect of the small but finite macroscopic elasticity, which can stem from a conservative interaction between particles or a finite Brownian motion: this elasticity can sometimes cause an instability [33].

## ACKNOWLEDGMENTS

MMD is happy to acknowledge a collaboration with Daniel Bonn, whose unpublished experimental data were an important stimulus to this work. Our code makes use of the CHOLMOD library by Tim Davis for direct Cholesky factorization of the sparse resistance matrix [34]. This research was supported in part by a grant of computer time from the City University of New York High Performance Computing Center under NSF CNS-0855217, CNS-0958379, and ACI-1126113. J.F.M. was supported in part by NSF PREM (DMR 0934206).

- 
- [1] A. B. Metzner and M. Whitlock, *Trans. Soc. Rheol.* **2**, 239 (1958).
  - [2] H. A. Barnes, *J. Rheol.* **33**, 329 (1989).
  - [3] E. Brown and H. M. Jaeger, *Rep. Prog. Phys.* **77**, 046602 (2014).
  - [4] E. Brown, N. A. Forman, C. S. Orellana, Z. Hanjun, B. W. Maynor, D. E. Betts, J. M. DeSimone, and H. M. Jaeger, *Nature Mater.* **9**, 220 (2010).
  - [5] G. V. Franks, Z. Zhou, N. J. Duin, and D. V. Boger, *J. Rheol.* **44**, 759 (2000).
  - [6] R. G. Egres, *The effect of particle anisotropy on the rheology and microstructure of concentrated colloidal suspensions through the shear thickening transition*, Ph.D. thesis, University of Delaware, Newark, DE (2005).
  - [7] A. Fall, N. Huang, F. Bertrand, G. Ovarlez, and D. Bonn, *Phys. Rev. Lett.* **100**, 018301 (2008).
  - [8] E. Brown and H. M. Jaeger, *Phys. Rev. Lett.* **103**, 086001 (2009).
  - [9] J. Mewis and N. J. Wagner, *Colloidal Suspension Rheology* (Cambridge University Press, 2011).
  - [10] M. Wyart and M. E. Cates, *Phys. Rev. Lett.* **112**, 098302 (2014).
  - [11] Z. Pan, H. de Cagny, B. Weber, and D. Bonn, arXiv:1412.5333 [cond-mat] (2014).
  - [12] A. Fall, F. Bertrand, D. Hautemayou, C. Mezière, P. Moucheront, A. Lemaître, and G. Ovarlez, *Phys. Rev. Lett.* **114**, 098301 (2015).
  - [13] N. A. Spenley, X. F. Yuan, and M. E. Cates, *J. Phys. II France* **6**, 551 (1996).
  - [14] P. Coussot, *Rheophysics: Matter in All Its States* (Springer, 2014).
  - [15] H. M. Laun, *J. Non-Newtonian Fluid Mech.* **54**, 87 (1994).
  - [16] W. J. Frith, P. d’Haene, R. Buscall, and J. Mewis, *J. Rheol.* **40**, 531 (1996).
  - [17] M. Neuville, G. Bossis, J. Persello, O. Volkova, P. Boustingory, and M. Mosquet, *J. Rheol.* **56**, 435 (2012).
  - [18] M. Grob, C. Heussinger, and A. Zippelius, *Phys. Rev. E* **89**, 050201 (2014).
  - [19] C. Heussinger, *Phys. Rev. E* **88**, 050201(R) (2013).
  - [20] N. Fernandez, R. Mani, D. Rinaldi, D. Kadau, M. Mosquet, H. Lombois-Burger, J. Cayer-Barrioz, H. J. Herrmann, N. D. Spencer, and L. Isa, *Phys. Rev. Lett.* **111**, 108301 (2013).
  - [21] R. Seto, R. Mari, J. F. Morris, and M. M. Denn, *Phys. Rev. Lett.* **111**, 218301 (2013).
  - [22] R. Mari, R. Seto, J. F. Morris, and M. M. Denn, *J. Rheol.* **58**, 1693 (2014).
  - [23] H. Nakanishi, S.-i. Nagahiro, and N. Mitarai, *Phys. Rev. E* **85**, 011401 (2012).
  - [24] R. C. Ball and J. R. Melrose, *Physica A* **247**, 444 (1997).
  - [25] D. J. Jeffrey and Y. Onishi, *J. Fluid Mech.* **139**, 261 (1984).
  - [26] D. J. Jeffrey, *Phys. Fluids A* **4**, 16 (1992).
  - [27] D. Bi, J. Zhang, B. Chakraborty, and R. P. Behringer, *Nature* **480**, 355 (2011).
  - [28] I. K. Ono, S. Tewari, S. A. Langer, and A. J. Liu, *Phys. Rev. E* **67**, 061503 (2003).
  - [29] P. D. Olmsted, *Europhys. Lett.* **48**, 339 (1999).
  - [30] P. D. Olmsted, *Rheol. Acta* **47**, 283 (2008).
  - [31] R. G. Egres and N. J. Wagner, *J. Rheol.* **49**, 719 (2005).
  - [32] P. T. Neno and E. D. Wetzal, *Smart Mater. Struct.* **23**, 125019 (2014).
  - [33] M. E. Cates, D. A. Head, and A. Ajdari, *Phys. Rev. E* **66**, 025202 (2002).
  - [34] <http://faculty.cse.tamu.edu/davis/suitesparse.html>